A hybrid model for particle transport and electron energy distributions in positive column electrical discharges using equivalent species transport

Fred Y. Huang[a] and Mark J. Kushner[b]
Department of Electrical and Computer Engineering, University of Illinois, 1406 West Green Street, Urbana, Illinois 61801

(Received 1 June 1995; accepted for publication 10 August 1995)

A new modeling technique for low-pressure, low-temperature discharges is introduced in which electrons, ions, and excited neutrals are equivalently treated using particle-mesh algorithms. Heavy particles are represented as electrons in bound states having large effective masses and the appropriate charge. An effective density of states is used which has discrete negative energies representing bound states, and a positive continuum representing free electrons. Collisions between continuum electrons and heavy particles are computationally treated as electron–electron collisions. This method has been used as the kinetic portion of a hybrid kinetic-fluid model for positive column electrical discharges. Densities and electric fields are obtained from the fluid portion of the model. Transport coefficients, source functions, and energy distributions for all species are generated in the kinetic module. The hybrid model has been used to examine electron energy distributions and radial electric fields in positive column discharges. Evidence is presented for diffusion heating of electrons in the sheaths. © *1995 American Institute of Physics.*

I. INTRODUCTION

Electron and ion transport in positive column electrical glow discharges has been investigated by a number of workers over the years.[1,2] There remains, however, a number of unresolved issues related to electron transport in the vicinity of the walls, and particularly in the sheaths, where the radial ambipolar electric fields may greatly exceed the applied axial electric field. The radial ambipolar electric fields are generated by the small charge separation produced by the transport of the more mobile electrons to the wall compared to the heavier ions. As a result, the plasma acquires a small net positive charge which is the origin of the term "electropositive" discharge.[3]

The fact that the ambipolar radial electric field in cylindrical positive column discharges is most often large compared to the applied axial electric field has motivated a number of investigations into its effect on the electron energy distribution (EED). The radial electric field can affect the EED in at least two ways. First, as electrons move radially toward the wall they perform work on the ambipolar field, thereby losing energy. Only electrons having a total kinetic energy which exceeds the local plasma potential relative to the wall can cross the sheath region to recombine at the wall. As a consequence, the EED near the wall is depleted of electrons with energies above this potential difference, a process termed "diffusion cooling."[4] Zhilinskii, Liventseva, and Tsendin[5] and Tsendin and Golubovskii[6] have computed radially dependent EEDs in a cylindrical positive column and determined that the EED is successively depleted above two energies. The first energy is the first inelastic collision threshold for excitation which produces a "cutoff" EED. The second energy is the wall potential energy, above which the tail of the EED is depleted due to losses resulting from diffusion cooling. This effect should be most prominent at radii $r>R-L_E$, where R is the radius of the discharge tube and L_E is the energy relaxation distance.

The second process for which the radial electric field affects the EED is, in a sense, the opposite of that just discussed. The process has been termed "diffusion heating" by Phelps.[3] The context of his discussion was to explain higher rates of ionization in positive column discharges then can be accounted for the axial electric field. In diffusion heating electrons at large radii, where the radial electric field is large compared to the axial electric field, are accelerated by the axial electric field to kinetic energies just below the ionization potential. They then move radially inward at nearly constant total energy, and are accelerated by the ambipolar electrical field above the ionization threshold. This change in trajectory can occur by an elastic momentum-transfer collision which results in a negligible change in energy. After undergoing the ionization collision, the lower-energy electron moves radially outward. The phenomenon of diffusion heating can be expected to be a sensitive function of the momentum and energy loss cross sections, and hence of gas mixture.

Several methods have been employed to calculate electron transport and EEDs in positive column glow discharges. The appropriate method depends on the value of λ_E/Λ, where λ_E is the electron mean free path and Λ is the classical diffusion length of the discharge tube. Small values of λ_E/Λ allow the use of the local field approximation (LFA) and fluid equations. Large values of λ_E/Λ require that a kinetic treatment be used. Hybrid models have generally had success at bridging the gap between these two approaches in simulating cathode falls and rf discharges. In hybrid simulations, a kinetic model is used to obtain nonequilibrium transport coefficients while a fluid model is used to obtain charge densities and the electric field. For example, Surendra, Graves, and Jellum[7] and Shoenbach, Chen, and Schaefer[8] developed self-consistent hybrid models for the cathode fall in dc dis-

[a]Electronic mail: f-huang@uiuc.edu
[b]Electronic mail: mjk@uiuc.edu

 0021-8979/95/78(10)/5909/10/$6.00

charges. Multidimensional hybrid models have been more recently applied to the analysis of inductively coupled plasma reactors for etching.[9]

In this article we introduce a new kinetic scheme for a hybrid model of positive column discharges called equivalent species transport (EST). In this algorithm, electrons and heavy particles are treated identically in a Monte Carlo simulation to resolve energy distribution functions (EDFs) and transport coefficients of all particles. The EST technique has been used as the kinetic module of a Monte Carlo fluid hybrid model for a cylindrical positive column discharge. In Sec. II the mechanics of the EST hybrid model are discussed. Results from the hybrid model for discharges sustained in He/N_2 and He/CF_4 gas mixtures are presented in Sec. III and IV. The results of this study have been used to investigate the influence of the radial electric field on the EED. We observed that the shape of the electron EED near the wall was a sensitive function of pressure. At higher pressures, diffusion cooling dominates, indicated by a decrease in average electron energy as one approaches the wall. At low pressures, diffusion heating effects become important, indicated by extrema in the average electron energy approaching the wall. Angular and energy distributions of electrons and ions incident on the radial wall of the discharge were investigated and the dependence of these distributions on pressure, gas composition, and *pd* (the product of the pressure and discharge tube diameter) product are discussed.

II. DESCRIPTION OF THE MODEL

The model used in the study is a hybrid simulation consisting of two modules. The first is a Monte Carlo simulation (MCS) using the EST method, while the second is a fluid module. The simulation begins with the kinetic module. We assume an initial particle density profile, and axial and radial electric fields. Trajectories of pseudoparticles in the MCS are advanced in these electric fields for a time $\Delta t_M \approx 1.5$ μs. Typically 25 000 pseudoparticles are employed. Source terms and transport coefficients for all species are calculated from the EDFs obtained from the MCS, which are then passed to the fluid module (FM). In the FM, continuity equations for all species and Poisson's equation are integrated using these quantities. The equations in the FM are typically integrated for $\Delta t_F \cong 1.5$ μs. The axial and radial electric fields obtained in the FM are passed to the MCS, and the process is iterated to convergence, as indicated by a steady state value of species densities and electric field. Once a quasisteady-state set of electric fields have been produced, additional iterations are performed to collect statistics. Typically, 30–50 total iterations are performed.

A. The Monte Carlo simulation and the equivalent species transport method

In many kinetics schemes used in hybrid models different methodologies are used to address different types of particles. For example, electrons are typically treated differently than heavy particles (ions and excited neutral states) when resolving their EDFs. From a computational viewpoint, it is expedient to separate these classes of particles since, for example, the time steps required to resolve their transport may differ, or their range of energies may be different. These classes of particles also differ in their density of states. Electrons in the discharge are energetically in a continuum. Heavy particles, on the other hand, exist in a continuum for translational energy, but also have internal degrees of freedom (that is, excited states). There are, however, advantages to consolidating all species into a single algorithm, particularly with respect to simplicity in implementing kinetic schemes in hybrid models. The implementation of multispecies kinetic modules on massively parallel computers would also benefit from using identical algorithms. One can achieve this consolidation of algorithms (that is, treating all species identically) by viewing excited (or for that matter ground) states of heavy particles as simply electrons in bound (or discrete) states. These "bound-state" electrons differ from continuum electrons by their density of states, effective masses, and effective charge. Consolidating particles in this fashion has precedent in solid-state electronics where electrons in the conduction band (the continuum) are represented by free electrons whereas electrons in the valence band (consisting of discrete states) are represented by holes having a different effective mass and charge.

To address this need for consolidation in gas discharges, we developed the EST method. The basis of the EST method is that all pseudoparticles, regardless of the real particles they represent, are mechanically treated identically. Each pseudoparticle is assigned a potential energy, represented by a density of discrete states, and a kinetic energy, represented by occupancy of a continuum state. Heavy particles (e.g., ground state and excited atoms) are represented by "bound electrons" or pseudoparticles which are in a discrete potential energy state in addition to their continuum translational kinetic energy. Unbound, or free electrons, are only in the kinetic continuum and have zero quantized potential energy. In principle, continuum electrons have positive energies of any value, while bound electrons exist in quantum states with negative energies. The zero point in this scale represents the threshold of the continuum.

Collisions between particles of any type are viewed as electron–electron collisions in which the collision partners undergo transitions between states. In an electron-impact excitation collision of heavy particles, the bound electron undergoes a transition to a state of less negative potential energy, whereas the free electron loses the appropriate amount of kinetic energy to conserve energy. For example, in electron-impact excitation of an argon atom, the bound electron makes a transition between the $3p^6$ and $3p^5\,4s$ states, while the free electron loses 10.9 eV of kinetic energy.

To obtain the EDF of the bound and free electrons, Boltzmann's equation is solved using Monte Carlo techniques,[10]

$$\frac{df}{dt} = -\frac{q\mathbf{E}}{m}\nabla_v \cdot f - \mathbf{v}\nabla_x \cdot f + \left(\frac{\partial f}{\partial t}\right)_c, \tag{1}$$

where f is the distribution function. Using the EST method, the collision operator of Boltzmann's equation then becomes

$$\left(\frac{\partial f_i}{\partial t}\right)_c = -\sum_{j=-1}^{-\infty} \langle f_i|\beta_i|f_j\rangle + \sum_{j=-1}^{-\infty}\sum_{k=1}^{\infty} \langle f_j|\beta_{jki}|f_k\rangle, \quad (2)$$

where β_{ij} represents the transition probability between electrons in states i and j, and β_{ijk} is the probability of yielding an electron in state k. The negative indices represent the bound states, while the positive indices represent continuum states dominantly populated by free electrons. Free electrons and bound-state electrons are distinguished by assigning effective masses, charges, and densities of states. Using this representation, free electrons and heavy particles are treated in a computationally identical fashion. Additional species can be generally added to the model without modification of the algorithm.

Although the EST method is, in principle, a simplification of the algorithms, there are practical matters which sometimes require special treatment. The free-electron density is typically much lower than, for example, vibrationally excited state densities in molecular gases, or metastable state densities in rare gases. One therefore has difficulty in resolving a large dynamic range of densities with a reasonable number of pseudoparticles. This issue is addressed by initially having pseudoparticles represent different numbers of real particles (called the pseudoparticle's weighting). The rate of generation of pseudoparticles of, for example, vibrationally excited states is also reduced by collecting statistics on the rate of excitation, and producing a smaller number of excited pseudoparticles having a larger weighting.

The MCS is initialized with a specified axial electric field, an electrically neutral selection of charged pseudoparticles whose spatial distribution is fundamental mode diffusion, and a radial ambipolar electric field in a cylindrical discharge tube. Although the MCS is three-dimensional, for the cases discussed here statistics have been collected only in the radial dimension. The initial velocities of the free electrons are randomly chosen from a 1 eV Maxwellian distribution, while the heavy particles are given thermal velocities. During the MCS, the trajectories of the psuedoparticles are advanced based on the accelerations produced by the local electric field. The details of the collisional Monte Carlo method used are discussed by Weng and Kushner.[10] A modified null collision method is used to account for changing collisional frequencies during a particle's time of flight resulting from both a change in the particle's energy and the density of the collision partners. As these collisions occur, particles may be created or removed, or they may change their state (corresponding to a different species). These collisions are summed thereby generating a source function $S_i(r)$ for each species i. An electron collision frequency is also obtained by summing collisions, thereby providing the particle's mobility. The electron-impact collisional cross sections are taken from the works of several authors.[10–22] Collisions between heavy particles use an energy-independent cross section derived either from a collisional rate coefficient, Lennard–Jones parameters,[23] or ion swarm data. The heavy particle collisions and rate coefficients used in the He/N_2 and He/CF_4 gas mixtures investigated in this work are listed in Refs. 24 and 25.

B. The fluid module

The fluid module generates species densities and electric fields as a function of position using the source functions and transport coefficients produced in the MCS. Densities are obtained by solving the continuity equation for each species,

$$\frac{\partial N_i}{\partial t} = -\nabla\cdot(q_i\mu_i\mathbf{E} - D_i\nabla N_i) + S_i, \quad (3)$$

where S_i is the source function obtained from the MCS, E is the radial electric field, μ is the particle mobility, q_i is the particle charge, and D_i is its diffusion coefficient. All charged species recombine on the cylindrical walls without secondary emission. The radial electric field is produced by solving a Poisson's equation for the electric potential,

$$\nabla^2\Phi = -\frac{\rho}{\epsilon_0}, \quad (4)$$

where ρ is the local charge density. The radial electric field is then obtained by $E_r = -\nabla_r\Phi$. Poisson's equation is formulated using a semi-implicit algorithm, described in Ref. 8. The resulting differential equation is solved by a simple inversion of the resulting tridiagonal matrix. The quasisteady-state axial electric field E_A is obtained by calculating the local conductivity σ and specifying a total current through the discharge tube,

$$E_A = \frac{I}{\int\sigma(r)dA}. \quad (5)$$

The radial and axial electric fields obtained at the end of the FM are transferred back to the MCS for use in the next iteration.

III. PLASMA PARAMETERS FOR He/N_2 POSITIVE COLUMN DISCHARGES

In this section we present results from the hybrid model for plasma parameters in N_2 and He/N_2 discharges for various gas pressures, gas compositions, and radius of the discharge tube. The densities of charged species as a function of radius are shown in Fig. 1(a) for our standard conditions: He/N_2=80/20, pressure of 100 mTorr, discharge tube radius of 2.5 cm, and total current of 500 mA (current density of 25.5 mA/cm^2). The radial electric field and electron temperature [defined as $T_e=(2/3)\langle\epsilon\rangle$] are shown in Fig. 1(b). The dominant ion is N_2^+ having a maximum density of $\approx 2.9\times10^9$ cm^{-3}. The density of He^+ has a maximum value of $\approx 5\times10^8$ cm^{-3}, whereas that of N^+ is small in comparison (and not shown in the figure). The large N_2^+ density results from its lower ionization potential compared to He, and the rapid rate of charge exchange between He^+ and N_2. Although the total plasma density is smooth, there is some noise in partitioning the densities between the ions. This results from the statistical nature of generating source functions in the MCS and the rapid rate of charge exchange between He^+ and N_2.

The separation between the presheath and sheath in a positive column discharge is somewhat ambiguous. In a classical plasma, the presheath is that region between a field-free neutral bulk plasma and the sheath. Ions are accelerated in the presheath to the Bohm velocity prior to entering a (col-

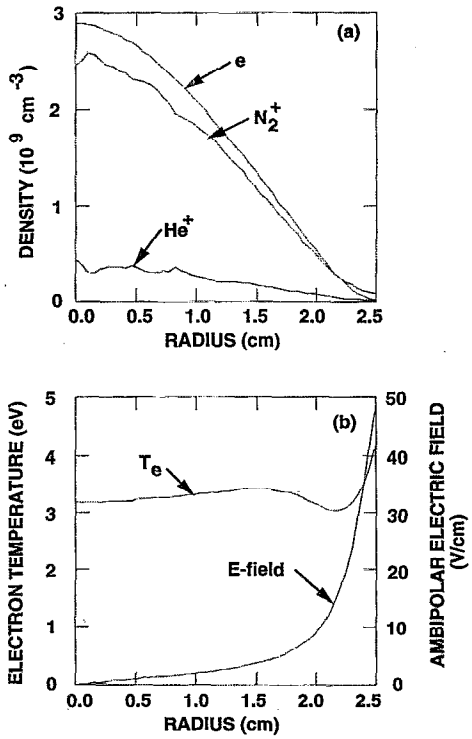

FIG. 1. Computed properties of a cylindrical positive column discharge for the standard conditions (He/N_2=80/20, 100 mTorr, 25.5 mA/cm^2 radius =2.5 cm). (a) Charged particle densities and (b) radial electric field and electron temperature. The presheath begins at ≈1.8 cm, and the sheath at 2.3 cm. The increase in electron temperature in the sheath is evidence of diffusion heating.

lisionless) sheath. In a bounded plasma, such as a positive column, the plasma is only field free on the axis. The ambipolar electric field continuously accelerates ions from the axis to the wall, usually in a collisional fashion, and the sheath itself may be collisional. In a sense, the presheath extends across the entire radius. For purposes of discussion, we define the sheath as starting at the radius where the charge density is visibly positive. The presheath is that region at smaller radii where the ambipolar electric field begins to significantly increase, but the plasma is still quasineutral. Using these definitions, in the standard case the presheath begins at a radius of ≈1.8 cm, whereas the sheath begins at a radius of ≈2.3 cm. The radial electric field is zero on the axis of the discharge due to symmetry considerations, moderately increases to ≈5 V/cm^{-1} at the edge of the presheath, and increases to ≈48 V/cm at the wall. The radial electric field is similar to that predicted by Metze *et al.*[2]

The electron temperature is ≈3.2 eV in the bulk plasma, but displays extrema at large radii. These extrema are sensitive functions of gas mixture and pressure, and appear to result from the opposing effects of diffusion cooling and heating. As discussed in Sec. I, diffusion cooling results from more energetic (and presumably more mobile) electrons breaching the potential barrier in the sheath, thereby reducing the average energy of the local EED. In diffusion heating electrons created with low energy or scattered radially inward in the sheath are accelerated by the sheath toward the center of the plasma, thereby increasing their energy. In our standard case, the electron temperature decreases in the presheath region, partly a consequence of diffusion cooling, but increases in the high-field region of the sheath near the wall. This increase in temperature is attributed to a diffusion heating phenomenon. The empirical observation from our parameterizations is that in gas mixtures containing significant amounts of N_2, the electron temperature is a function of both the axial and radial electric fields.

The fact that the electron temperature may increase in the sheath is counterintuitive since the electric field in that region opposes the net motion of electrons toward the wall. Recall that the power which sustains the ambipolar electric field and accelerates ions through the presheath and sheath originates from the axial electric field which raises the electron temperature above that of the ion temperature. The requirement that must be met is that the net (volume-averaged) power resulting from radial transport of the electrons be negative. That is, work must be performed by the electrons on the ambipolar field, which is then transferred to the ions. This requirement is

$$\int (\mathbf{j}_e \cdot \mathbf{E})_r d^3r = \int [(qD\nabla n + q\mu n\mathbf{E})_r \cdot \mathbf{E}_r] d^3r < 0. \quad (6)$$

For demonstration purposes, let us assume that we have fundamental mode diffusion in a parallel-plate geometry having width L. For these conditions, the electron density and radial ambipolar electric fields are (keeping terms to first order)

$$n = n_0 \cos\left(\frac{\pi x}{L}\right), \quad (7a)$$

$$E_r = -\frac{kT_e}{q}\left(1 - \frac{D_I}{D_e}\right)\frac{\nabla n}{n}. \quad (7b)$$

Substituting Eq. (7) into Eq. (6), one can show that the equivalent requirement on the electron temperature and mobility to sustain the radial ambipolar electric field is

$$-\frac{4n_0}{qL}\left(\frac{\pi}{L}\right)^2 \int_0^{L/2} \mu_I k T_I \left(1 - \frac{\mu_I T_I}{\mu_e T_e(x)}\right) \frac{\sin^2\left(\frac{\pi x}{L}\right)}{\cos\left(\frac{\pi x}{L}\right)} dx < 0. \quad (8)$$

So an electron temperature which increases in the sheath is not inconsistent with the requirements for sustaining the ambipolar electric field and will actually increase the net power transferred to the ions. A decreasing T_e in the sheath regions (that is, diffusion cooling) reduces the net power transferred to the ions.

The conditions which must be met in order that the electron temperature increases with increasing radius are that the acceleration of inward directed electrons between energy loss collisions exceed the average energy of the outward directed electrons. Radially inward directed electrons are accelerating from the average energy to higher energies, whereas radially outward electrons are decelerating from the average energy to lower energies. We therefore require a momentum transfer cross section which decreases with increasing energy above the average electron temperature.

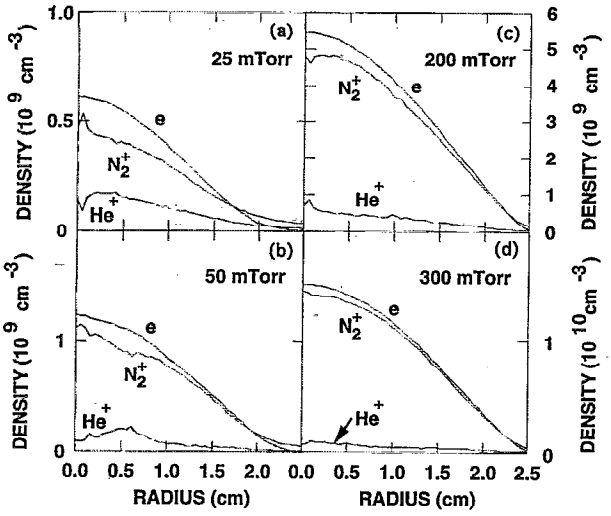

FIG. 2. Charged particle densities for cylindrical positive column discharges (He/N_2=80/20, 25.5 mA/cm^2, radius=2.5 cm) for different pressures: (a) 25 mTorr; (b) 50 mTorr; (c) 200 mTorr; and (d) 300 mTorr. The electron density increases with increasing gas pressure to maintain a constant current density at the higher collision frequency.

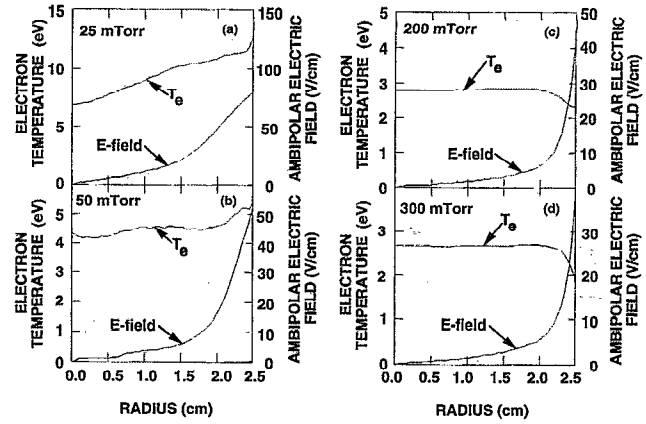

FIG. 3. Electron temperature and radial electric field for the conditions of Fig. 2: (a) 25 mTorr; (b) 50 mTorr; (c) 200 mTorr; and (d) 300 mTorr. The increasing electron temperature in the sheaths at the lower pressure results from a diffusion heating effect. The electron temperature decreases in the sheaths at the higher pressures, an indication of diffusion cooling.

We investigated whether the results for T_e shown in Fig. 1(b) may be a numerical artifact. For example, the order of the integration was increased and the fraction of a mesh cell a pseudoparticle may cross in any time step was decreased. Both of these procedures reduced but did not eliminate the effect. In the approach to the steady state, it is often necessary to add more pseudoparticles to account for an imbalance between ionization and loss. Electron pseudoparticles which "appear" in the sheath region will be accelerated toward the center of the tube. We reduced this effect by gathering final statistics only after a convincing steady state had been reached. The effect could be emphasized by the fact that we may not be fully resolving the sheath. For example, a very thin sheath would simply act as a high-pass energy filter which reflects the lower-energy electrons. Such an arrangement would not affect the EED other than "cutting it off" at the sheath potential. There are, however, 5–10 computational mesh points in the non-neutral region and so the majority of the sheath structure is being resolved.

Plasma densities, electron temperatures and radial electric fields are shown in Figs. 2 and 3 for a pressure range of 25–300 mTorr but otherwise having the same conditions as the standard He/N_2 case. The electron densities increase nearly linearly with pressure, as expected, since the current density is held constant while the mobility decreases with increasing pressure. Although the axial E/N (electric field/number density) does decrease with increasing gas pressure, this effect is not large enough to compensate for the decrease in mobility. At low pressure, the plasma density appears diffusion dominated. At higher pressures above 300 mTorr the plasma densities in the inner portions of the discharge begin to slightly flatten, creating a shallow plateau. This may indicate that recombination is an increasingly more important ion loss mechanism.

The radially averaged electron temperature increases with decreasing gas pressure in order to increase the ionization rate to offset the larger diffusion losses. The sheath thickens with decreasing pressure and plasma density (0.2 cm at 300 mTorr to 0.75 cm at 20 mTorr). In doing so, the net electric field in the discharge increases as a larger fraction of the volume is occupied by the presheath and sheath. The end result is that diffusion heating appears to dominate at low pressures (electron temperature increases with increasing radius), whereas at high pressure, diffusion cooling dominates (electron temperature decreases with increasing radius).

The phenomenon of diffusion heating can be restated as the electron temperature being a function of the magnitude of the local electric field (axial plus radial) as opposed to being a function of only the axial electric field. Experimental evidence for diffusion heating can be found in studies by Sudit[26] in which Langmuir probe measurements of EEDs in a N_2 positive column discharge were made as a function of radius. The experimental conditions are 20 mTorr, with a discharge current of 200 mA and a radius of 7.6 cm. Our simulation of EEDs as a function radius for Sudit's experimental conditions are shown in Fig. 4(a). The experimentally measured EEDs are reproduced in Fig. 4(b). For comparison, EEDs in N_2 using the local field approximation calculated using a two-term spherical harmonic solution to Boltzmann's equation are shown in Fig. 5 as function of E/N. The computed results of the hybrid simulation agree very well with those for the measured EEDs throughout the discharge. In all cases (experimental and theoretical), the EED near the center of the discharge tube is "cut-off," as is characteristic of an electron swarm in N_2 at low axial E/N ($<$100 Td as shown in Fig. 5). Near the wall in Fig. 4, where the axial E/N is unchanged, but the total magnitude of the electric field has increased, the EED is characteristic of an electron swarm at high E/N ($>$100 Td as shown in Fig. 5). The electron temperature, as obtained from an average over the EEDs, increases with increasing radius in the experiments as shown in Fig. 6. This trend of increasing T_e with radius indicates a diffusion heating mechanism.

The degree of heating of the EEDs in regions of large

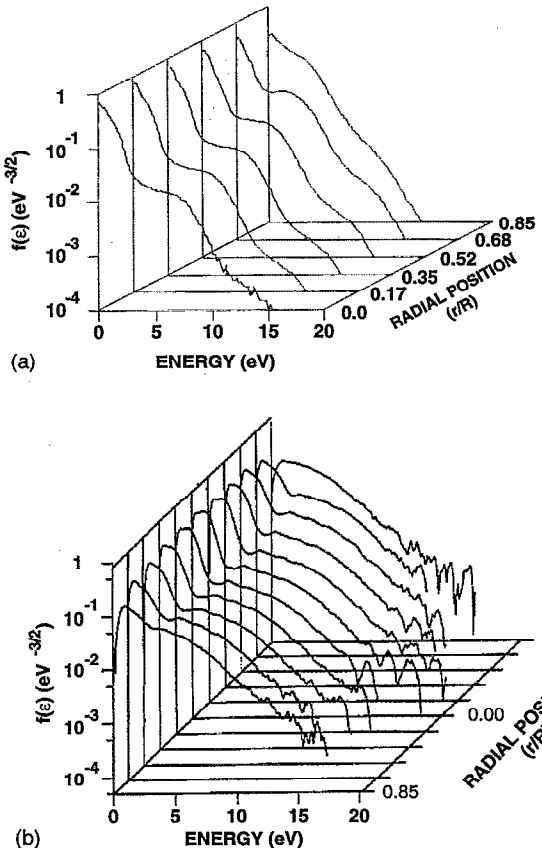

FIG. 4. Computed and experimental EEDs at different radii for a N_2 discharge operating at a *pd* product of 0.15 Torr cm. (a) Computed values; (b) experimental EEDs, reproduced from Ref. 26. Note that the experimental results span the entire diameter of the discharge tube. The decrease in the experimental EED near zero energy is an artifact of the measurement. In both cases, the EED near the wall is characteristic of a high E/N compared to the EED near the axis.

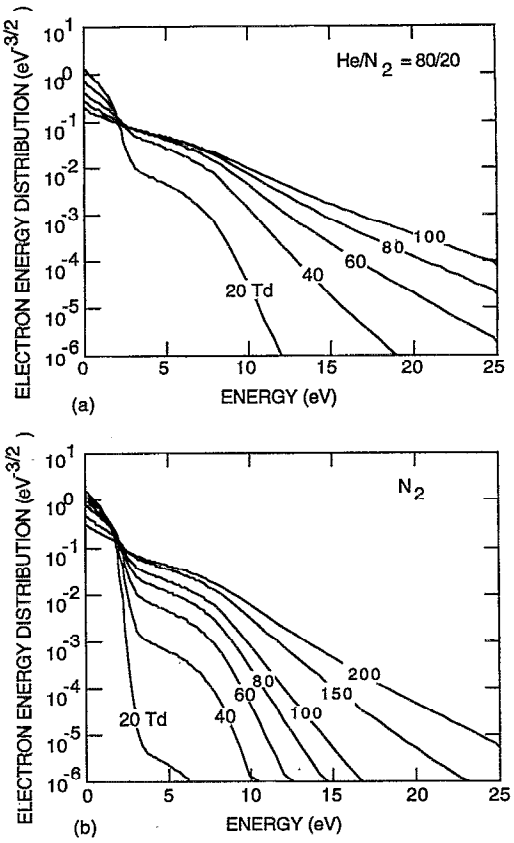

FIG. 5. EEDs for various values of E/N (1 Td=10^{-17} V cm^2): (a) He/Ne$_2$=80/20 and (b) N_2. These EEDs, obtained by solution of Boltzmann's equation using a two-term spherical harmonic expansion, are for a uniform applied electric field. The shape of the EEDs at large radii calculated with the hybrid model and observed experimentally resemble those obtained at large E/N.

radial electric fields is a function of gas mixture. This dependence is shown in Fig. 7 where EEDs are plotted near the axis and near the wall in gas mixtures ranging from He/N_2=80/20 to 20/80. Radial electric fields and electron temperatures are shown in Fig. 8 for the same conditions. Charged particle densities are shown in Fig. 9. The bulk electron temperature decreases with increasing N_2 fraction, in response to the larger rate of momentum transfer and energy loss to vibrational excitation. The radial electric field and sheath potential also commensurately decreases since both of these quantities are proportional to electron temperature. The local maximum in electron temperature as a function of radius is larger in the N_2 rich gas mixtures, while the diffusion heating is more severe with the N_2 lean mixtures. This trend may, in fact, be more a function of the larger electric field in the sheaths than the gas mixture. In all cases, the EED near the wall is characteristic of an electron swarm at high E/N, whereas that at the center of the tube is characteristic of an electron swarm at low E/N. The disparity between EEDs at the center of the tube and the wall increases with increasing N_2 mole fraction. This may be expected since the shape of the EED is less sensitive to changes in E/N over the range of interest for He compared to N_2. Due to the lower ionization threshold for N_2 compared to He, and the rapid rate of charge exchange from He^+ to N^+ and N_2^+ (k=1.3×10^{-9} cm^3 s^{-1}) the N_2^+ density is always large compared to the He^+ densities.

A common parameter for analyzing positive column discharges is *pd*, the product of the gas pressure and the diameter of the discharge tube. As this parameter increases, we expect a lower rate of diffusion losses, a smaller ambipolar field, a smaller axial field, and a lower electron temperature. We parameterized the model for a He/N_2=80/20 gas mixture keeping the values of *pd* and total current constant while varying the pressure and diameter. The results are shown in

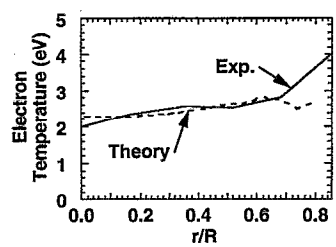

FIG. 6. Experimental and computed electron temperature as a function of radius for the conditions of Fig. 4.

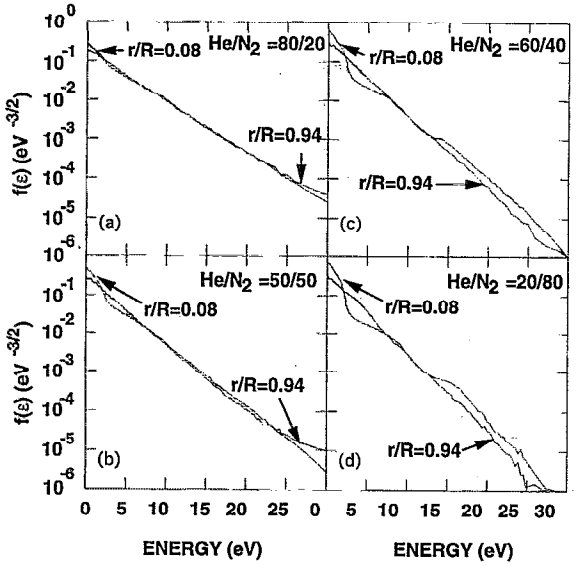

FIG. 7. EEDs at large and small radii for various gas mixtures: (a) He/N_2=80/20; (b) He/N_2=50/50; (c) He/N_2=60/40; and (d) He/N_2=20/80. The disparity in the shape of the EED between the center and the edge of the discharge is greatest in gas mixtures which are rich in N_2.

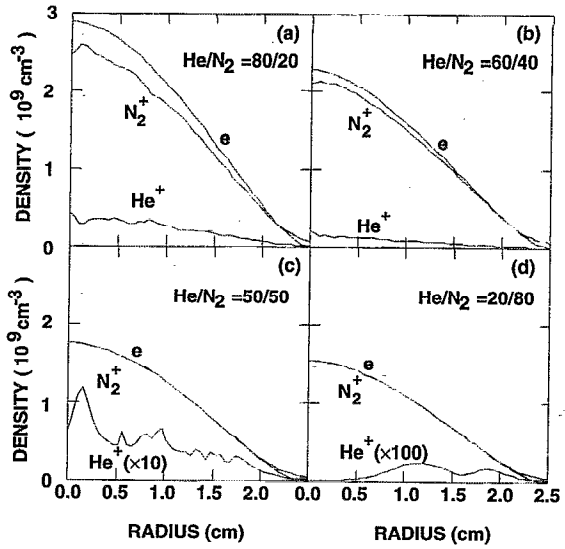

FIG. 9. Charge densities as a function of radius for various gas mixtures: (a) He/N_2=80/20; (b) He/N_2=50/50; (c) He/N_2=60/40; and (d) He/N_2=20/80. The He^+ density is small in the N_2-rich mixtures.

Fig. 10 for pd=0.5 cm Torr (167 mTorr, 3.0 cm diameter; 100 mTorr, 5 cm diameter). The magnitudes of the axial and radial electric fields, and the bulk electron temperatures are essentially the same in both cases. At 500 mA, the discharges have current densities of 25.5 and 70.7 mA/cm^2, respectively. The expected ratio of electron densities (small tube/large tube) based on maintaining $\int j\,dA$ constant is 1.66, which is essentially the ratio obtained in the simulations. We find, however, that the diffusion heating near the wall is not identical in the two cases, and is more significant at the lower pressure. Note that the ambipolar electric field is a function of electron temperature, which scales with pd and not pressure. The E/N in the sheaths is therefore larger at the lower pressure even though pd is a constant. The diffusion heating appears to be function of the higher net E/N in the sheaths since the ratio of the electron means free path to the thickness of the sheath is the same in both cases.

The energy and angular distribution of particles striking the wall were investigated, and examples of that study appear in Fig. 11 where the energy distributions for electrons, N_2^+ and He^+, are shown for the standard case. The ion energy distributions (IEDs) extend to a maximum energy of 15 eV, which is the maximum plasma potential. Ions having this energy originate at the center of the tube, and strike the wall

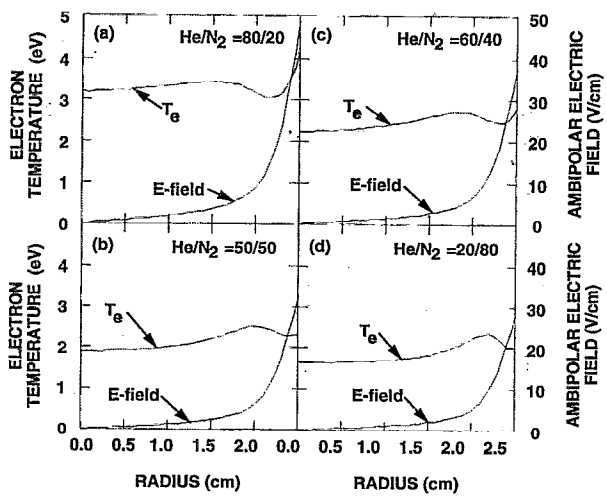

FIG. 8. Electron temperature and radial electric field as a function of radius for various gas mixtures: (a) He/N_2=80/20; (b) He/N_2=50/50; (c) He/N_2=60/40; and (d) He/N_2=20/80. The electron temperature and magnitude of the radial electric field decrease with increasing N_2 fraction, although the sheath thickness does not appreciably change.

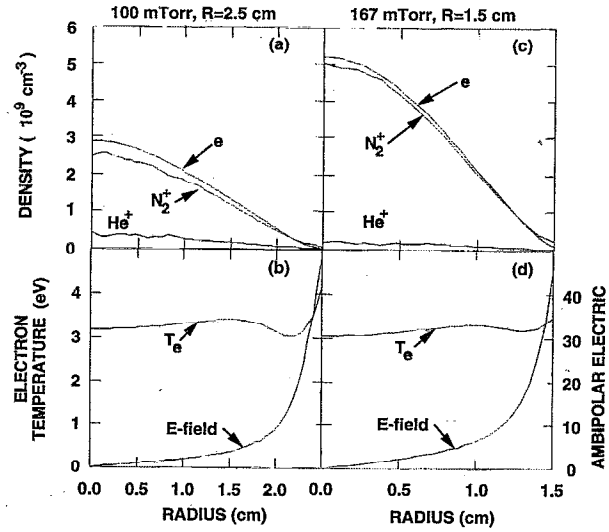

FIG. 10. Computed properties for two He/N_2 discharges with pd value of 0.5 Torr cm. (a) Charged species densities and (b) electron temperature and radial electric field for a 100 mTorr, 2.5-cm-radius discharge. (c) Charged species densities and (d) electron temperature and radial electric field for a 167 mTorr, 1.5-cm-radius discharge.

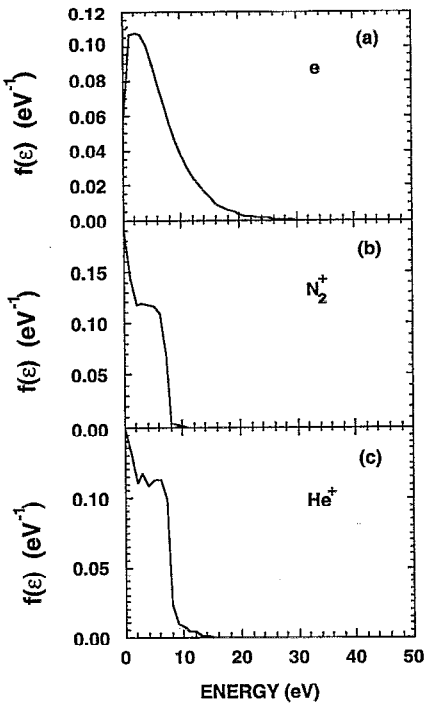

FIG. 11. Energy distributions of charged particles striking the radial wall for the standard conditions (He/N_2=80/20, 100 mTorr): (a) electrons; (b) N_2^+; and (c) He^+. The ion energies extend to the maximum plasma potential.

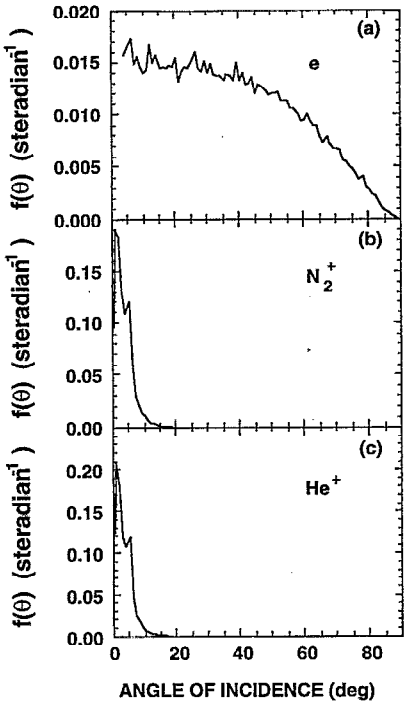

FIG. 12. Angular distribution of charged particles striking the radial wall for the standard conditions (He/N_2=80/20, 100 mTorr): (a) electrons; (b) N_2^+; and (c) He^+. The ion angles are forward peaked, reflecting their acceleration through the sheath. The electron angles of incidence are essentially isotropic.

having gained an energy nearly equal to the full plasma potential of energy. The IED appears to be "cut-off"≈9 eV. This cutoff corresponds to ions which are thermal when entering the sheath, but collisionlessly (or nearly so) traverse the sheath. This portion of the IED appears to be the superposition of two distributions. The first results from the "free flight" of ions just described. The second is a "thermal" distribution of low energies which represents ions created in the sheath or having experienced charge exchange reactions deep into the sheath. The EED striking the wall extends to higher energies, indicative of their bulk distributions.

The angular distributions (ADs) striking the wall are shown in Fig. 12. The ADs for the heavy ion particles are anisotropic, having a width of ≈10°. The ADs result from the nearly collisionless ion acceleration through the sheaths. The ADs for both He^+ and N_2^+ have similar structure. The low-angle peak corresponds to the free-flight ions whereas the high angle peak and tail correspond to the thermal ions. The AD for electrons is nearly isotropic. Electrons which reach the wall are only decelerated in the direction normal to the wall by the ambipolar field. This deceleration can, at best, preserve the AD of electrons from the bulk and at worst broaden it.

IV. PLASMA PARAMETERS FOR He/CF_4 DISCHARGES

Discharges sustained in helium and carbon tetrafluoride were chosen to investigate electronegative gas mixtures. The standard case used in this study is He/CF_4=90/10 at a pressure of 100 mTorr. The discharge current is 750 mA with a tube radius of 2.5 cm (current density of 38.2 mA/cm^2).

Charged particle densities as a function of radius are shown in Fig. 13. The electron temperature and ambipolar electric field are shown in Fig. 14(a). The distributions are qualitatively different than for the electropositive He/N_2 cases. In the bulk plasma, the ratio $[F^-]/[e]>6$. Charge neutrality with positive ions is dominantly maintained by the negative ions. The dominant loss mechanisms for electrons are dissociative attachment to CF_4 and dissociative recombination with CF_3^+. The end result is that the ambipolar electric field is small in the bulk "electronegative" portion of the plasma. The electronegative region extends to ≈1.8 cm where the presheath begins. At this radius, the ambipolar electric field increases, producing a sufficiently large plasma potential to exclude the

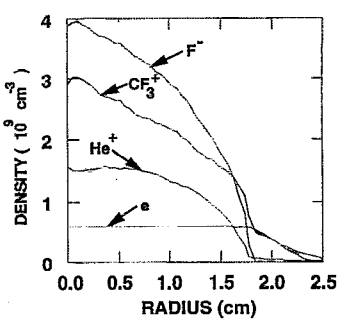

FIG. 13. Charged particle densities as a function of radius for a He/CF_4=90/10 gas mixture (100 mTorr). Charge neutrality is maintained largely by negative ions in the bulk plasma.

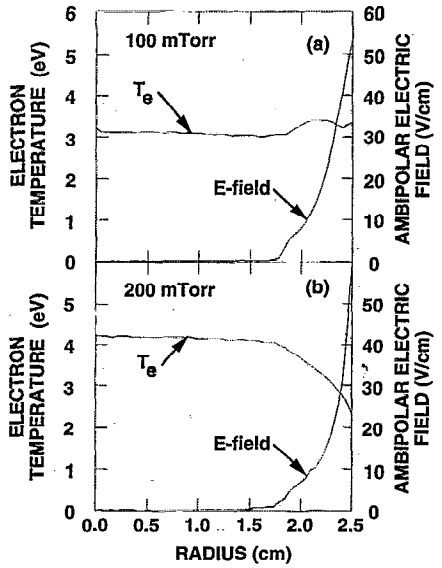

FIG. 14. Electron temperature and radial electric field for a discharge in a He/CF_4=90/10 gas mixture: (a) 100 mTorr and (b) 200 mTorr. The electric field is small in the bulk plasma where the negative ion density is large. Note that at the lower pressure, diffusion cooling dominates.

cold negative ions. At larger radii, charge neutrality is maintained largely by electrons and CF_3^+. The electron temperature is essentially constant as a function of radius, with some evidence of diffusion heating in the sheath.

The electron temperature and radial electric field are shown in Fig. 14(b) for a gas pressure of 200 mTorr. The electric field is qualitatively similar to that at lower pressure;

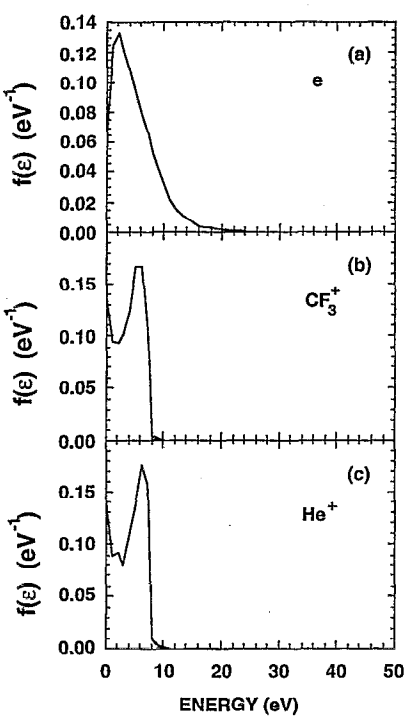

FIG. 15. Energy distributions of charged particles striking the radial wall for the conditions of Fig. 13: (a) electrons; (b) CF_3^+; and (c) He^+.

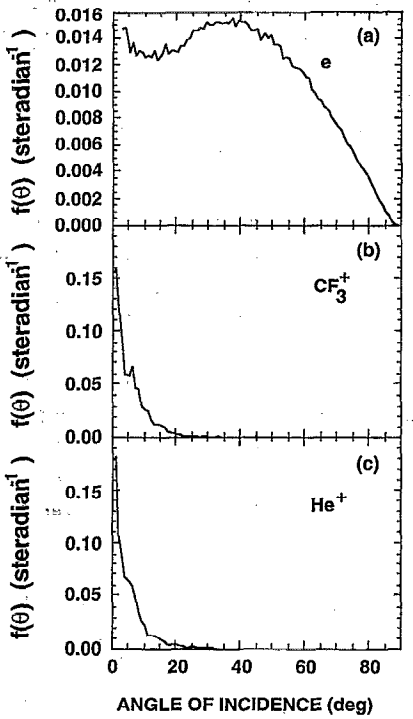

FIG. 16. Angular distribution of charged particles striking the radial wall for the conditions of Fig. 13: (a) electrons; (b) CF_3^+; and (c) He^+.

small at radii interior to the presheath in regions where charge neutrality is maintained by negative ions. The electron temperature, however, decreases in and near the sheaths, an indication of diffusion cooling at the higher pressure.

Energy distributions for particles striking the wall of the discharge are shown in Fig. 15. They have the same general characteristics as for the He/N_2 electropositive discharges. The IEDs in the electronegative discharge, though, are more highly peaked at the energies corresponding to ions free falling from the edge of the sheath. This results from two effects: First, the sheath is somewhat thinner, thereby allowing more free-flight trajectories; second, the rates of charge exchange for both CF_3^+ and He^+ are lower in the He/CF_4 mixture. CF_3^+ does not undergo exothermic ion–molecule collisions with He or CF_4 at ambient temperatures, while the rate coefficient for charge exchange of He^+ with CF_4 is significantly less than for N_2. The larger proportion of ions having energies in the peak near 10 eV produces angular distributions which are more highly peaked in the forward direction, as shown in Fig. 16.

V. CONCLUDING REMARKS

A new modeling technique for simulating low-temperature plasmas has been developed and incorporated into a hybrid Monte Carlo fluid model. This method, termed the equivalent species transport method, treats all species of interest equivalently by defining an effective density of states. The model has been applied to analysis of electropositive and electronegative cylindrical discharges where the magnitudes of the radial electric field in the presheath and sheath are large compared to the applied axial electric field.

We found that the EED for these conditions is a function of radius, and hence a function of the net electric field (applied axial electric field plus ambipolar electric field). In He/N_2 and N_2 discharges, the shape of the EED in the center of the plasma is essentially what one would expect for the applied axial E/N. The EED in the sheath regions has a shape corresponding to a higher E/N, although less than the magnitude of the net electric field. Computed EEDs which show this heating agree well with probe measurements made by Sudit[26] in N_2 positive column discharges.

The "hot" EEDs at large radii produce, under some conditions, an electron temperature which increases with increasing radius. This may be evidence for a diffusion heating phenomena, described by Phelps.[2] There appear to be three regimes which characterize average energy as a function of radius. At high pressures ($\lambda_E \ll R$, λ_E is the electron mean free path) T_e will be nearly constant as a function of radius. At intermediate pressures ($\lambda_E \approx R$), diffusion cooling will occur and T_e may decrease in the sheaths. At low pressures ($R > \lambda_E > L$, L is the sheath thickness), diffusion heating may occur and T_e may increase in or near the sheaths. When $\lambda_E \geqslant R$, T_e is once again spatially uniform. Diffusion heating is a sensitive function of gas mixture and pressure, but is not necessarily a function of E/N in the sheath. A requirement for diffusion heating is that the mean free path for energy loss be comparable to or exceed the sheath thickness.

ACKNOWLEDGMENTS

This work was supported by the Semiconductor Research Corporation, the National Science Foundation, and the University of Wisconsin ERC for Plasma Aided Manufacturing. The authors would like to thank A. Phelps for discussions on positive column discharges and I. Sudit for access to his experimental data prior to publication.

[1] J. H. Ingold, in *Gaseous Electronics*, edited by M. N. Hirsh and H. J. Oskam (Academic, New York, 1978), p. 2, and references therein.
[2] A. Metze, D. W. Ernie, and H. J. Oskam, Phys. Rev. A **39**, 4117 (1989).
[3] A. V. Phelps, J. Res. Nat. Inst. Stand. Technol. **95**, 407 (1990).
[4] M. Biondi, Phys. Rev. **93**, 1136 (1954).
[5] A. P. Zhilinskii, I. F. Liventseva, and L. D. Tsendin, Sov. Phys. Tech. Phys. **22**, 177 (1977).
[6] L. D. Tsendin and Yu. B. Golubovskii, Sov. Phys. Tech. Phys. **22**, 1066 (1977).
[7] M. Surendra, D. B. Graves, and G. M. Jellum, Phys. Rev. A **41**, 1112 (1990).
[8] K. H. Schoenbach, H. Chen, and G. Schaefer, J. Appl. Phys. **67**, 154 (1990).
[9] P. L. G. Ventzek, R. J. Hoesktra, and M. J. Kushner, J. Vac. Sci. Technol. B **12**, 461 (1994).
[10] Y. Weng and M. J. Kushner, Phys. Rev. A **42**, 6192 (1990).
[11] J. P. Boeuf and E. Marode, J. Phys. D **15**, 2169 (1982).
[12] W. C. Fon, K. A. Berrington, P. G. Burke, and E. A. Kingston, J. Phys. B **13**, 2309 (1980).
[13] M. Hayashi, in *Swarm Studies and Inelastic Electron–Molecule Collisions*, edited by L. C. Pitchford, B. V. McKoy, A. Chutjian, and S. Trajmar (Springer, New York, 1987), pp. 167–187.
[14] W. L. Borst, Phys. Rev. A **5**, 648 (1972).
[15] D. C. Cartwright, S. Trajmar, A. Chutjian, and W. Williams, Phys. Rev. A **16**, 1041 (1977).
[16] R. T. Brinkman and S. Trajmar, Ann. Geophys. **26**, 201 (1970).
[17] L. Vriens, Phys. Lett. **8**, 260 (1964).
[18] J. B. A. Mitchell, Phys. Rep. **186**, 215 (1990).
[19] Y. Itikawa, M. Hayashi, A. Ichimura, K. Onda, K. Sakimoto, K. Takayanagi, M. Nakamura, H. Nishimura, and T. Takaynagi, J. Phys. Chem. Ref. Data **15**, 985 (1986).
[20] R. H. Schultz and P. B. Armentrout, Proc. Int. J. Mass Spec. Ion. **107**, 29 (1991).
[21] L. C. Pitchford and A. V. Phelps, Phys. Rev. A **25**, 540 (1982).
[22] M. Ohuchi and T. Kubota, J. Phys. D **16**, 1705 (1983).
[23] R. A. Svehla, NASA Technical Report R-132, 1962, p. 1.
[24] T. J. Sommerer and M. J. Kushner, J. Appl. Phys. **71**, 1654 (1992).
[25] F. Huang, M. S. thesis, University of Illinois at Urbana-Champaign, 1994.
[26] I. Sudit, Ph.D. thesis, University of Wisconsin-Madison, 1993, Chap. 5.